Eur. Phys. J. B **47**, 369–378 (2005)
DOI: 10.1140/epjb/e2005-00342-9

THE EUROPEAN PHYSICAL JOURNAL B

Ab initio many-body treatment of the electronic structure of metals

O. Peschel[1], I. Schnell[2], and G. Czycholl[1,a]

[1] Department of Physics, University of Bremen, PO Box 330 440, 28334 Bremen, Germany
[2] Theoretical Division, Los Alamos National Laboratory, Los Alamos, New Mexico 87545, USA

Received 6 May 2005 / Received in final form 15 July 2005
Published online 28 October 2005 –

Abstract. We propose and apply a combination of an ab initio (band-structure) calculation with a many-body treatment including screening effects. We start from a linearized muffin-tin orbital (LMTO) calculation to determine the Bloch functions for the Hartree one-particle Hamiltonian, from which we calculate the static susceptibility and dielectric function within the standard random phase approximation (RPA). From the Bloch functions we obtain maximally localized Wannier functions, using a method proposed by Marzari and Vanderbilt. Within this Wannier basis all relevant one-particle and unscreened and screened Coulomb matrix elements are calculated. This yields a multi-band Hamiltonian in second quantization with ab initio parameters, for which screening has been taken into account within the simplest standard approximation. Then, established methods of many-body theory are used. We apply this concept to a simple metal, namely lithium (Li). Here the maximally localized Wannier functions turn out to be of the sp^3-orbital kind. Furthermore, only the on-site contributions of the screened Coulomb matrix elements are relevant, and a generalized, four-band Hubbard model is justified. The screened on-site Coulomb matrix elements are considerably smaller than the band width because of which it is sufficient to calculate the selfenergy in weak-coupling approximation. We compare results obtained within the screened Hartree-Fock approximation (HFA) and within the second-order perturbation theory (SOPT) in the Coulomb matrix elements for Li and find that many-body effects are small but not negligible even for this simple metal.

PACS. 71.10.Fd Lattice fermion models (Hubbard model, etc.) – 71.15.Ap Basis sets (LCAO, plane-wave, APW, etc.) and related methodology (scattering methods, ASA, linearized methods, etc.) – 71.15.Mb Density functional theory, local density approximation, gradient and other corrections – 71.20.Dg Alkali and alkaline earth metals

1 Introduction

Most existing ab initio (first-principles) methods for the numerical calculation of the electronic properties of solids are based on density functional theory (DFT) [1–3]. But as the functional dependence of the kinetic energy and the exchange and correlation part of the Coulomb (interaction) energy on the electron density are not known explicitly, additional approximations are necessary. Here the most common and successful method is the local density approximation (LDA) [4], which assumes that the exchange-correlation potential depends locally on the electronic density and makes an ansatz for the exchange-correlation functional, which is based on the homogeneous electron gas. Such DFT-LDA calculations have been very successful for many materials and ground-state properties such as crystal structure, ground state and ionization energy, lattice constant, etc. However, there are also important limitations. For example, LDA predicts a band gap for semiconductors that is almost a factor of two too small, and for many strongly correlated (narrow energy band) systems such as high-temperature superconductors, heavy fermion materials, transition-metal oxides, and $3d$ itinerant magnets, the LDA is usually not sufficient for an accurate description (predicting metallic rather than semiconducting behavior, failing to predict quasi-atomic-like satellites, etc.). For such systems, better justified many-body theories [5] have to be used, but these methods have to be applied to a second quantized Hamiltonian.

Until recently such application of many-body methods was restricted to model Hamiltonians with adjustable parameters for which at most order of magnitude estimates were available. Therefore, the application of true many-body methods and ab initio methods were distinct approaches in solid-state theory. But within the past decade, there have been several attempts to combine ab initio and many-body methods [6–13]. Most successful in this respect has been the application of the "dynamical mean-field theory" (DMFT) [14] for the treatment of the

[a] e-mail: czycholl@itp.uni-bremen.de

correlation problem; these LDA+DMFT approaches [11–13] are reviewed in references [15,16]. Most of the mentioned work starts from a standard DFT/LDA ab initio calculation, from which one obtains the one-particle band structure. Then estimates on the local, screened Coulomb (Hubbard) matrix elements U between localized orbitals are made, for which the "constrained LDA" (CLDA) [17,18] is usually used. The resulting (extended) multi-band Hubbard model (with ab initio one-particle bands and CLDA estimates for the Hubbard U's) is then treated within many-body approximations, either standard (diagrammatic) ones like second order perturbation theory (SOPT) [7] or "fluctuation exchange approximation" (FLEX) [9] or the DMFT [14,15].

Another possibility to take into account many-body effects beyond LDA and screening in ab initio electronic structure calculations is provided by the GW approximation (GWA); [19] for recent reviews see references [20,21]. The GWA is an approximation for the selfenergy diagrammatically corresponding to the exchange contribution but with a dynamically screened interaction line. A full GW calculation requires the knowledge of the frequency dependent dielectric function and, therefore, of the one-particle states over a large energy range [22]. Within GWA the screened interaction is frequency dependent, i.e. dynamic. Therefore, within GWA effective (extended) Hubbard models with static, short ranged Coulomb matrix elements (Hubbard U etc.) cannot be derived, one automatically obtains a model with an effective dynamical, frequency dependent interaction $U(\omega)$. Combinations of GWA and DMFT have been developed and applied to correlated systems like Ni only very recently [23].

In this paper we suggest and apply a slightly different, alternative approach. As the LDA contains already some aspects of (exchange and) correlations (in form of the ansatz for the local exchange correlation potential) and the correlations shall be treated in a better justified many-body theory, we do not use the LDA at all, but start from an ab initio Hartree calculation. The solution of the effective one-particle Schrödinger equation yields the Hartree band structure and the eigenstates (in the form of Bloch functions). The eigenenergies (band structure) allow for a calculation of the static susceptibility or the static dielectric function in the most simple approximation, namely the (static) random phase approximation (RPA or generalized Lindhard approximation). From the Bloch functions we can calculate maximally localized Wannier functions using an algorithm proposed by Marzari and Vanderbilt [24]. Within these Wannier functions one can calculate all one-particle (tight-binding) matrix elements of the (second-quantized) Hamiltonian and also – using the static dielectric function obtained – the screened Coulomb (two-particle) matrix elements. Then one has the Hamiltonian in second quantization in form of a multi-band, generalized Hubbard model and can apply many-body methods. This approach differs from our earlier investigations [25,26] in that we now calculate screened Coulomb matrix elements (which turn out to be automatically short ranged). In contrast to the GWA [23] we take into account only static (and not dynamic) screening and derive an effective (Hubbard) Hamiltonian with statically screened interaction matrix elements (Hubbard U's). True many-body theory (with the possibility of the calculation of a frequency dependent, dynamic selfenergy beyond the RPA or GWA) is applied to this effective Hamiltonian. This has, in particular, the advantage that we have to calculate only the static dielectric constant and, therefore, do not need the basis functions in an energy regime of unoccupied bands etc. [22].

To demonstrate the feasibility of this suggested approach we apply it to a simple metal, namely lithium (Li). Here the $2s$- and $2p$-bands are the relevant bands which determine the electronic structure and which in Hartree approximation we calculate using a standard band structure method, namely the "linearized muffin tin orbital" (LMTO) method [27,28]. The maximally localized Wannier functions turn out to be of the sp^3-orbital form, and with respect to these orbitals we obtain four (almost) degenerate hybridized $2sp$-bands. For the one-particle (tight-binding) matrix elements contributions up to the fifth neighbor have to be taken into accout to reproduce the band structure. Whereas the unscreened Coulomb matrix elements turn out to be relatively large even for such a simple metal (of the order of 13 eV for the on-site intraband, 10 eV for the on-site interband and still 4−5 eV for the nearest-neighbor matrix elements), the screened Coulomb matrix elements are considerably smaller, namely on-site matrix elements of the order of 2−5 eV and negligibly small intersite matrix elements. Therefore, Li is described by a four-band extended Hubbard model with (up to fifth neighbor) tight-binding matrix elements and only local on-site (inter- and intra-band) Coulomb matrix elements. None of these matrix elements are free adjustable parameters; they are all determined "from first principles". Then many-body approximations can be applied. As the screened Hubbard U's are small compared to the band width, a weak-coupling many-body approximation is justified just for Li, and we present and compare results obtained within the (screened) Hartree-Fock approximation (HFA) with results obtained within the simplest HFA-extension, namely the SOPT.

The paper is organized as follows. In Section 2 we describe the Hartree approximation, the results for the Hartree band structure of Li and for the static (generalized Lindhard) susceptibility. Section 3 presents and discusses the maximally localized Wannier functions and their properties. Results for the matrix elements are given in Section 4; here we describe, in particular, how the (screened) Coulomb matrix elements can be calculated using fast Fourier transformation (FFT) and present results for the unscreened and screened Coulomb matrix elements. The resulting Hamiltonian in second quantization is studied in HFA and SOPT as the simplest weak-coupling many-body methods, which are described in Sections 5 and 6. SOPT-results for the selfenergy and the density of states are presented in Section 6 and compared with (screened) HFA results before the paper closes with a short conclusion.

2 Hartree approximation and dielectric function

We start from an ab initio Hartree calculation, i.e. we solve the effective one-particle Schrödinger equation

$$(H_0 + V_{\mathrm{H}}(\mathbf{r}))\,\varphi_{n\mathbf{k}}(\mathbf{r}) = \varepsilon_n(\mathbf{k})\varphi_{n\mathbf{k}}(\mathbf{r}). \tag{1}$$

Here

$$H_0 = -\frac{\hbar^2}{2m}\nabla^2 + V(\mathbf{r}) \tag{2}$$

is the one-particle part of the Hamiltonian with $V(\mathbf{r})$ the (periodic) lattice potential and

$$V_{\mathrm{H}}(\mathbf{r}) = \int d^3r' \frac{e^2 n(\mathbf{r}')}{|\mathbf{r}-\mathbf{r}'|} \tag{3}$$

denotes the Hartree potential with the particle density

$$n(\mathbf{r}) = \sum_{n\mathbf{k}\sigma}^{\mathrm{occ.}} |\varphi_{n\mathbf{k}}(\mathbf{r})|^2. \tag{4}$$

Here we prefer the Hartree approximation to the LDA because the effects of exchange and correlation shall be taken into account by the application of the many-body methods to the second-quantized Hamiltonian. Therefore, it is not necessary (and avoids possible double counting) to include exchange and correlation effects on the level of the effective one-particle Schrödinger equation by means of an approximate exchange-correlation potential.

As the particle density depends on the one-particle wave functions $\varphi_{n\mathbf{k}}(\mathbf{r})$ to be determined, equation (1) forms a selfconsistency problem to be solved by iteration. The one-particle quantum numbers $(n\mathbf{k}\sigma)$ denote the band index, the wave vector (from the first Brillouin zone) and the spin. The one-particle Schrödinger equation (1) can be solved using any of the established numerical band-structure calculation methods. Just for simplicity and convenience we use the "linearized muffin tin orbital" (LMTO) method within the "atomic sphere approximation" (ASA) [27,28], which replaces the true potential within one unit cell by a spherically symmetric potential within a sphere of the same volume as that of the unit cell. This allows a classification of all states in terms of their angular momentum (l, s-, p-, d-, ...) contributions. But any other established band structure method, for instance the better justified full potential methods, can be used here.

Results obtained for the Hartree band structure of Li are shown in Figure 1 and compared with the corresponding LDA band structure. Here a bcc-lattice with a lattice constant of 3.5 Å $\approx 6.6a_0$ has been assumed, where a_0 denotes the Bohr radius as natural length scale when using atomic Rydberg units (ARU); then the Wigner-Seitz radius used in the ASA is $r_s = 3.25a_0$. Though the bcc-lattice is not as closed packed as an fcc-lattice, for which the ASA is usually good, the bcc-structure is also not as open that corrections to the ASA (in form of "empty spheres" etc.) are important. Furthermore, it is not our aim to perform the best possible band structure calculation, but we want to demonstrate the feasibility of the proposed combination of band structure and many-body calculations, and for that purpose any band structure method can be used. From Figure 1 we see that at least for this simple metal the Hartree and LDA result differ only in an almost constant energy shift caused by the (Barth-Hedin [29]) exchange correlation potential taken into account in LDA and neglected in the Hartree calculation. Therefore, relative to the chemical potential, the LDA and Hartree result are almost identical. Note that here (in contrast to the standard convention in band structure plots) we do not choose the chemical potential as the zero of our energy scale; the chemical potentials (Fermi levels) of the Hartree and LDA calculation are indicated as horizontal straight lines in Figure 1.

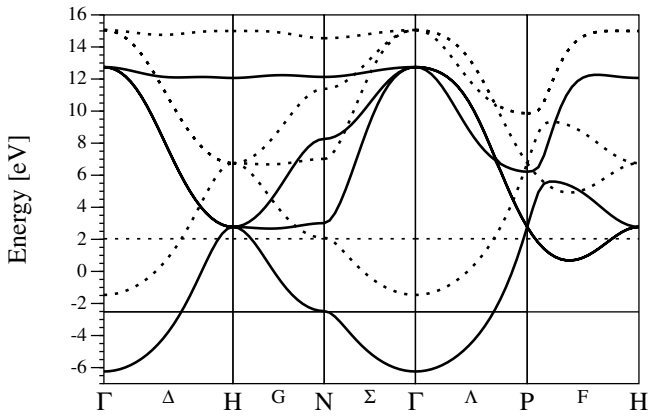

Fig. 1. Hartree band-structure (dashed line) and LDA band structure (full line) of Li; the horizontal straight lines indicate the Fermi levels of the Hartree (dashed line) and LDA (full line) calculation.

From this band structure, the static susceptibility and the dielectric function can be calculated within the generalized Lindhard theory or (static) RPA according to

$$\chi(\mathbf{q}) = \frac{2e^2}{V}\sum_{n,n',\mathbf{k}} \frac{f(E_{n\mathbf{k}}) - f(E_{n'\mathbf{k}+\mathbf{q}})}{E_{n\mathbf{k}} - E_{n'\mathbf{k}+\mathbf{q}}} |M_{n,n'}(\mathbf{k},\mathbf{q})|^2 \tag{5}$$

with

$$M_{n,n'}(\mathbf{k},\mathbf{q}) = \langle n'\mathbf{k}+\mathbf{q}|\mathrm{e}^{i\mathbf{q}\mathbf{r}}|n\mathbf{k}\rangle. \tag{6}$$

Obviously, because of the energy denominator in equation (5) the dominant contributions to $\chi(\mathbf{q})$ stem from transitions from occupied to unoccupied states close to the Fermi energy; therefore, the summation over the band indices n, n' in (5) can be restricted to the $2s$-, $2p$-bands kept in the LMTO calculation. Then the static dielectric function can be obtained from

$$\epsilon(\mathbf{q}) = 1 - \frac{4\pi}{q^2}\chi(\mathbf{q}). \tag{7}$$

This approach to calculate the susceptibility and the dielectric function is similar to the calculations of the dielectric function necessary for GWA treatments [22]. But as we perform an ab initio calculation only for the static

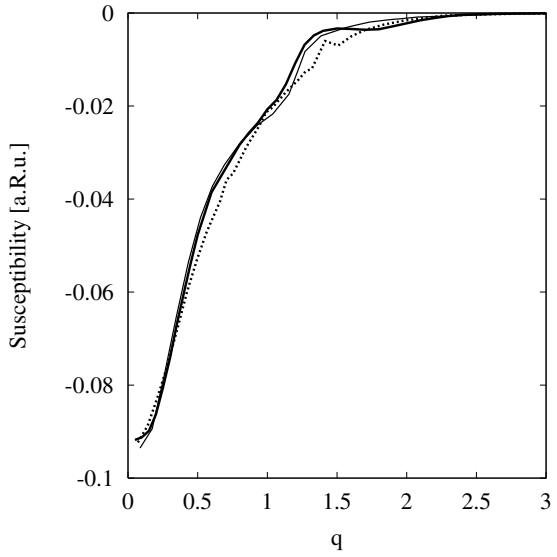

Fig. 2. q-dependence of static susceptibility for different **q**-directions, $\mathbf{q} = q(100)(\Delta)$ (thick line), $\mathbf{q} = q(110)(\Sigma)$ (dotted line), $\mathbf{q} = q(111)(\Lambda)$ (thin full line).

(q-dependent) susceptibility and dielectric function, we do not need an extended basis set with basis functions from a large energy range, but the (LMTO) basis set obtained for the (Hartree or LDA) band structure calculation is also sufficient for the calculation of $\chi(\mathbf{q})$. For a calculation of the dynamic (frequency ω dependent) susceptibility also transitions between (occupied and empty) states with an energy difference ω are important so that a considerable larger number of bands have to be considered and projections of the high energy sector on the low energy sector as in reference [23] would be necessary. But for the static susceptibility the high energy sector does not contribute. As mentioned in the introduction, the main difference of our approach to the standard GWA [19,21,23] is that we start by taking into account only static screening, obtain an effective Hamiltonian with statically screened, short-ranged Coulomb matrix elements and apply many-body theory to this effective Hamiltonian and can then take into account dynamic (frequency dependent) selfenergies beyond the RPA (GWA) diagram.

To obtain $\chi(\mathbf{q})$ numerically directly from (5), the $\mathbf{k}$ mesh must be sufficiently fine, especially for small $\mathbf{q}$. The main effort lies in the calculation of the matrix elements $M_{n,n'}(\mathbf{k},\mathbf{q})$, for which the explicit Bloch functions obtained in the solution of the eigenvalue problem (1) have to be used.

The dependence of $\chi(\mathbf{q})$ (also measured in ARU) on $|\mathbf{q}|$ is shown in Figure 2. The three lines show the result for different $\mathbf{q}$-directions, namely $\mathbf{q} = q(100)(\Delta)$, $q(110)(\Sigma)$, and $\mathbf{q} = q(111)(\Lambda)$. Obviously, $\chi(\mathbf{q})$ is not isotropic but (slightly) depends on the $\mathbf{q}$-direction. But the anisotropy is weak, i.e. $\chi(\mathbf{q})$ mainly depends only on the absolute value $|\mathbf{q}|$ and strongly decreases with increasing $|\mathbf{q}|$, as it is also known from the static Lindhard susceptibility of the homogeneous electron gas.

3 Maximally localized Wannier functions

One of our goals is the first-principles determination of the parameters of the electronic Hamiltonian in second quantization. For that purpose one has to start from a suitable one-particle basis, for which we choose the (maximally localized) Wannier functions. The Wannier states are related to the Bloch states by the unitary transformations:

$$w_{\mathbf{R}n}(\mathbf{r}) = \langle \mathbf{r}|\mathbf{R}n\rangle = \frac{1}{N}\sum_{\mathbf{k}} e^{-i\mathbf{k}\mathbf{R}}\psi_{n\mathbf{k}}(\mathbf{r})$$

$$|\psi_{n\mathbf{k}}\rangle = \sum_{\mathbf{R}} e^{i\mathbf{k}\mathbf{R}}|\mathbf{R}n\rangle. \tag{8}$$

Using the algorithm proposed by Marzari and Vanderbilt [24] maximally localized Wannier functions can be calculated from the LMTO Bloch wave functions, as described in reference [25]. Since the original Bloch functions are given in terms of a spherical harmonics expansion, the new Wannier functions (and their contribution in each individual muffin-tin sphere) can also be decomposed into these spherical harmonics contributions. Therefore, one can decompose the Wannier function localized at site $\mathbf{0}$ into its contributions in the different muffin-tin spheres also at other sites $\mathbf{R} \neq \mathbf{0}$ according to

$$w_{n\mathbf{0}}(\mathbf{r}) = \sum_{\mathbf{R}} w_{n\mathbf{0}}(\mathbf{R};\mathbf{r}) \tag{9}$$

where on the right hand side $\mathbf{r}$ varies only in the unit cell (muffin-tin sphere) around $\mathbf{R}$. Each component around site $\mathbf{R}$ can be decomposed into its different spherical harmonics contributions

$$w_{n\mathbf{0}}(\mathbf{R};\mathbf{r}) = \sum_{lm} \phi_l^{\mathbf{R}n}(r) Y_{lm}(\vartheta,\varphi). \tag{10}$$

As described in reference [26] one can calculate the weight of the contributions to the Wannier function (centered at $\mathbf{0}$) within the different muffin-tin spheres

$$\langle w_{n\mathbf{0}}|w_{n\mathbf{0}}\rangle_{\mathbf{R}} \equiv \int_{\mathbf{R}} d^3\mathbf{r}|w_{n\mathbf{0}}(\mathbf{R};\mathbf{r})|^2 \tag{11}$$

and one can decompose this into the different l-contributions according to:

$$\langle w_{n\mathbf{0}}|w_{n\mathbf{0}}\rangle_{\mathbf{R}} = \sum_l C_l^{\mathbf{R}n}. \tag{12}$$

For the simple metal Li it is sufficient to explicitly take into account only the $2s$- and $2p$-states, i.e. the l-summation is restricted to $l = 0, 1$. In Table 1 we summarize the properties of the maximally localized Wannier functions by giving their l-composition and their contribution in the central ($\mathbf{0}$-) unit cell (muffin-tin sphere, around which the Wannier function is localized), the nearest neighbor sites and within the further sites. As we start from a basis of four states (one $2s$- and three $2p$-states) per spin direction and $\mathbf{k}$, we obtain also four different (orthonormalized) Wannier functions per site and

Table 1. Properties of the four maximally localized Wannier functions for Li.

n	l	$C_l^{\mathbf{0}n}$	$\sum_{\mathbf{R}n.n.} C_l^{\mathbf{R}n}$	$\sum_{\mathbf{R}>n.n.} C_l^{\mathbf{R}n}$	$\sum_{\mathbf{R}} C_l^{\mathbf{R}n}$
0	s	0.240219	0.007837	0.000352	0.248408
	p	0.727476	0.022392	0.001723	0.751592
	Σ	0.967695	0.030229	0.002076	1.000000
1	s	0.240609	0.007837	0.000351	0.248797
	p	0.727083	0.022400	0.001720	0.751203
	Σ	0.967692	0.030237	0.002071	1.000000
2	s	0.240649	0.007837	0.000351	0.248837
	p	0.727042	0.022401	0.001719	0.751163
	Σ	0.967692	0.030238	0.002070	1.000000
3	s	0.240529	0.007837	0.000351	0.248717
	p	0.727164	0.022398	0.001721	0.751283
	Σ	0.967693	0.030235	0.002072	1.000000

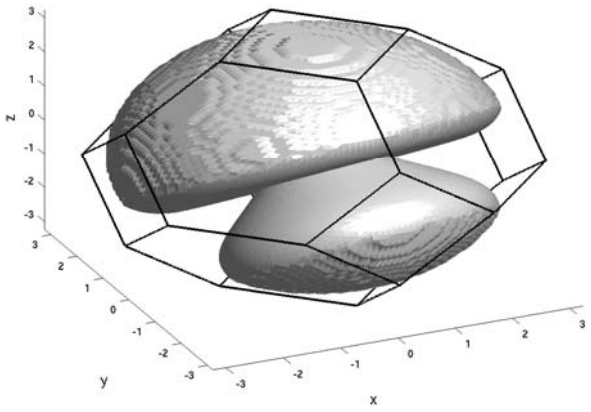

Fig. 3. Three dimensional isosurface plot of the squared Wannier function $|w_n(\mathbf{r})|^2$ (i.e. probability density for electron in one Wannier function) within central unit cell $\mathbf{0}$ (position of the atom); the Wigner-Seitz cell for the bcc-crystal is also sketched.

spin direction. We see from the table that about 97% of the total weight of each of the four Wannier functions is to be found already within the central unit cell; this shows how properly well localized our Wannier functions are. Furthermore, all four Wannier functions have about 25% s- and 75% p-character. The maximally localized Wannier functions generated by the Marzari-Vanderbilt algorithm are automatically of the hybridized sp^3-type, and as the "tails" within the other unit cells are almost negligible, they correspond essentially to the atomic (or molecular) sp^3-orbitals. This is demonstrated in Figure 3, which shows a 3-dimensional isosurface plot of one of the four Wannier functions $|w_{n\mathbf{0}}(\mathbf{r})|^2$ within a central unit cell (muffin tin sphere); here the atom sits at the origin, atomic units (of the Bohr radius $a_0 \approx 0.5$ Å) are used as the length scale, and the Wigner-Seitz cell for the bcc-structure is also sketched. The other three Wannier functions are equivalent but oriented into different, tetrahedron space directions.

4 One particle and Coulomb matrix elements

From the optimally localized Wannier functions one can calculate the one-particle matrix elements

$$t_{12} = \int d^3\mathbf{r}\ w_1^*(\mathbf{r}) H_0 w_2(\mathbf{r}) \tag{13}$$

and the unscreened Coulomb matrix elements

$$W_{12,34} = \int d^3\mathbf{r}\ d^3\mathbf{r}'\ w_1^*(\mathbf{r})\ w_2^*(\mathbf{r}')\ \frac{e^2}{|\mathbf{r}-\mathbf{r}'|}\ w_3(\mathbf{r}')\ w_4(\mathbf{r}). \tag{14}$$

Here we use the abbreviated notation $1, 2$ to mean $\mathbf{R}_1 n_1$, $\mathbf{R}_2 n_2$, etc. In reference [25] it is described how these matrix elements can be evaluated. Concerning the Coulomb matrix elements, we use the fast Fourier transformation (FFT) algorithm proposed in reference [25]. Using

$$\int d^3\mathbf{q}\ \frac{e^{i\mathbf{q}\mathbf{r}}}{\mathbf{q}^2} = \frac{2\pi^2}{|\mathbf{r}|} \tag{15}$$

one finds

$$W_{12,34} = \frac{e^2}{2\pi^2} \int \frac{d^3\mathbf{q}}{\mathbf{q}^2}\ f_{14}(\mathbf{q}) f_{23}(-\mathbf{q}) \tag{16}$$

$$f_{ij}(\mathbf{q}) \equiv \int d^3\mathbf{r} e^{i\mathbf{q}\mathbf{r}} w_i^*(\mathbf{r}) w_j(\mathbf{r}). \tag{17}$$

The f_{ij} functions are just the Fourier transforms of a product of Wannier functions. These can be obtained very efficiently by calculating the Wannier functions on a cubic mesh in real space and then applying a standard FFT algorithm.

This form (16) also easily allows for the calculation of (statically) screened Coulomb matrix elements using the dielectric constant calculated according to (7):

$$W_{12,34}^{sc} = \frac{e^2}{2\pi^2} \int \frac{d^3\mathbf{q}}{\epsilon(\mathbf{q})\mathbf{q}^2}\ f_{14}(\mathbf{q}) f_{23}(-\mathbf{q}). \tag{18}$$

For Li results for the one-particle, the unscreened and the screened Coulomb matrix elements are presented in the following tables.

We see from Table 2 that the one-particle part H_0 of the Hamiltonian has intra-band and inter-band matrix elements, i.e. it is not diagonal with respect to the band indices of the maximally localized Wannier functions. From the site diagonal matrix elements one clearly sees the equivalence of the four band indices of the sp^3-like Wannier basis. The nearest and next-nearest neighbor matrix elements do not show this symmetry because these matrix elements are given for one special nearest and next-nearest neighbor lattice vector. Furthermore we see that the site off-diagonal one-particle matrix elements decrease with increasing distance, i.e. the tight-binding assumption to neglect the inter-site (hopping) matrix elements for larger lattice vector distances is justified. But a nearest neighbor tight-binding model assumption is not sufficient, it turned out that taking into account the hopping matrix elements up to the fifth neighbors is a reasonably good approximation.

Table 2. Interband and intraband one particle matrix elements (in units of eV) $t_{\mathbf{R}nm} = \langle \mathbf{R}n|H_0|\mathbf{0}m\rangle$ for $\mathbf{R} = 0$ (on-site), $\mathbf{R} = (0.5, 0.5, 0.5)$ (nearest neighbor) and $\mathbf{R} = (1, 0, 0)$ (next nearest neighbor).

on-site				
$n =$	$m = 0$	1	2	3
0	–1.68	–0.41	–0.41	–0.41
1	–0.41	–1.68	–0.41	–0.41
2	–0.41	–0.41	–1.68	–0.41
3	–0.41	–0.41	–0.41	–1.68
nearest neighbors				
$n =$	$m = 0$	1	2	3
0	0.87	–0.79	–0.89	–2.23
1	0.31	–0.40	–0.20	–0.55
2	0.28	–0.15	–0.39	–0.47
3	–0.44	–0.47	0.38	–0.40
next nearest neighbors				
$n =$	$m = 0$	1	2	3
0	0.07	–0.28	0.15	–0.35
1	0.01	0.10	–0.02	0.07
2	0.03	–0.43	0.27	–0.53
3	0.00	0.13	–0.05	0.20

Table 3. Unscreened on-site direct $W_{\mathbf{0}n\mathbf{0}m,\mathbf{0}m\mathbf{0}n}$, on-site exchange $W_{\mathbf{0}n\mathbf{0}m,\mathbf{0}n\mathbf{0}m}$, and nearest neighbor direct $W_{\mathbf{0}n\mathbf{R}m,\mathbf{R}m\mathbf{0}n}$ Coulomb matrix elements calculated according to equation (16).

on-site direct Coulomb matrix elements				
$n =$	$m = 0$	1	2	3
0	13.16	10.13	10.12	10.13
1	10.13	13.17	10.12	10.12
2	10.12	10.12	13.17	10.12
3	10.13	10.12	10.12	13.17
on-site exchange matrix elements				
$n =$	$m = 0$	1	2	3
0	13.16	1.01	1.01	1.01
1	1.01	13.17	1.01	1.01
2	1.01	1.01	13.17	1.01
3	1.01	1.01	1.01	13.17
direct nearest neighbor Coulomb matrix elements				
$n =$	$m = 0$	1	2	3
0	4.53	3.80	3.77	3.50
1	5.11	4.44	4.21	3.88
2	5.17	4.28	4.44	3.91
3	6.35	4.86	4.82	4.48

Table 3 gives some of the unscreened two-particle Coulomb matrix elements. We see that the on-site, intraband matrix elements (essentially corresponding to the "Hubbard U") are largest, of the magnitude 13 eV, the on-site direct interband matrix elements are slightly smaller, of the magnitude 10 eV, and the exchange matrix elements are of the magnitude of 1 eV. As expected the nearest neighbor direct Coulomb matrix elements are smaller than the on-site ones but still of the magnitude 4−6 eV and, therefore, by no means negligible. Therefore, when working with unscreened Coulomb matrix elements one has to go far beyond nearest neighbors and, therefore, a very large number of (direct and exchange) Coulomb matrix elements has to be considered.

Table 4. Screened on-site direct $W^{sc}_{\mathbf{0}n\mathbf{0}m,\mathbf{0}m\mathbf{0}n}$, on-site exchange $W^{sc}_{\mathbf{0}n\mathbf{0}m,\mathbf{0}n\mathbf{0}m}$, and nearest neighbor direct $W^{sc}_{\mathbf{0}n\mathbf{R}m,\mathbf{R}m\mathbf{0}n}$ Coulomb matrix elements calculated according to equation (16).

on-site direct Coulomb matrix elements [eV]				
$n =$	$m = 0$	1	2	3
0	4.63	2.36	2.36	2.36
1	2.36	4.63	2.36	2.36
2	2.36	2.36	4.63	2.36
3	2.36	2.36	2.36	4.63
on-site exchange matrix elements				
$n =$	$m = 0$	1	2	3
0	4.63	0.80	0.80	0.80
1	0.80	4.63	0.80	0.80
2	0.80	0.80	4.63	0.80
3	0.80	0.80	0.80	4.63
nearest neighbor ($\mathbf{R} = (0.5, 0.5, 0.5)$) direct				
$n =$	$m = 0$	1	2	3
0	0.07	0.00	0.00	–0.01
1	0.13	0.03	0.01	0.00
2	0.14	0.02	0.03	0.01
3	0.48	0.09	0.08	0.04

When one takes into account static screening and calculates the screened Coulomb matrix elements according to (18) using the approximations (7, 5) one obtains the results tabulated in Table 4. As expected, the screened Coulomb matrix elements are considerably smaller than the unscreened ones. We now get about 4.6 eV for the intra-band and 2.4 eV for the interband direct on-site Coulomb matrix elements. The screened inter-site matrix elements are now negligibly small. This means that a generalized four-band Hubbard model can be really justified now when using the screened Coulomb matrix elements.

5 Hartree, unscreened and screened Hartree-Fock approximation

After we have determined the matrix elements within our restricted basis set of 4 maximally localized Wannier functions (per site and spin), we have a Hamiltonian in second quantization of the form

$$H = \sum_{12\sigma} t_{12} c^\dagger_{1\sigma} c_{2\sigma} + \frac{1}{2} \sum_{1234\sigma\sigma'} W_{12,34} c^\dagger_{1\sigma} c^\dagger_{2\sigma'} c_{3\sigma'} c_{4\sigma}. \quad (19)$$

In praxis some further truncation is necessary, because one cannot determine really all matrix elements in Wannier representation. Rather the one-particle matrix elements t_{12} will be explicitly evaluated only for a few neighbor shells, and also not all possible $(4N)^4$ Coulomb matrix elements can be calculated but a restriction to the most important ones is necessary. The explicit calculations yield that only Coulomb matrix elements like $W_{12,12}$ or $W_{12,21}$, for which at least two of the four indices pairwise agree, are of considerable magnitude. Furthermore also these rapidly

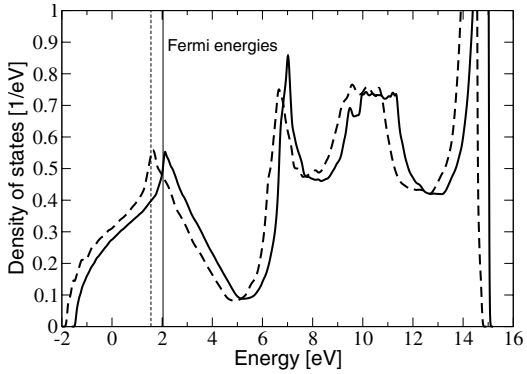

Fig. 4. Density of states in Hartree approximation in first quantization (full line) and in second quantization (dashed line); the vertical (full and dashed) lines indicate the position of the Fermi energy in the two calculations.

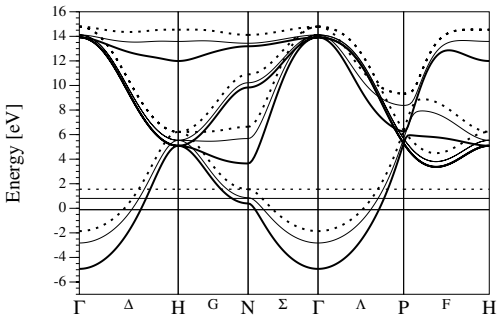

Fig. 5. Second quantized Hartree (dashed line), screened Hartree-Fock (thin line) and unscreened Hartree-Fock (thick full line) band structure; the corresponding straight lines parallel to the abscissa indicate the Fermi energy for the three band structures.

decrease with increasing distance $|\mathbf{R}_1 - \mathbf{R}_2|$ so that also the (unscreened) Coulomb matrix elements have to be considered only for a few neighbor shells. The simplest approximation one can now apply to the second quantized Hamiltonian (19) is again the Hartree approximation (HA). In second quantization HA means the replacement of (19) by the effective one-particle Hamiltonian:

$$H_{\mathrm{HA}} = \sum_{12\sigma} \left(t_{12} + \Sigma_{12}^{\mathrm{HA}}\right) c_{1\sigma}^{\dagger} c_{2\sigma} \tag{20}$$

$$\text{with} \quad \Sigma_{12}^{\mathrm{HA}} = \sum_{34\sigma'} W_{13,42} \langle c_{3\sigma'}^{\dagger} c_{4\sigma'} \rangle. \tag{21}$$

Here the expectation values $\langle c_{3\sigma'}^{\dagger} c_{4\sigma'} \rangle$ have to be determined self-consistently for the Hartree Hamiltonian (20). A simple diagrammatic analysis shows that in any case the Hartree term has to be evaluated with the unscreened Coulomb matrix elements (16). For the direct, density-density interaction entering the Hartree contributions, the interaction line has not to be renormalized, whereas in all higher diagrams (occurring in the diagrammatic perturbation theory with respect to the Coulomb interaction) renormalizations of the interaction lines and, therefore, the replacement of the bare Coulomb matrix elements (16) by the screened Coulomb matrix elements (18) is justified.

The effective Hamiltonian (20) in HA should, of course, reproduce the result of the first quantized Hartree calculation (1), from which we started off applying the band structure (LMTO) method and from which we obtained our one-particle basis and our matrix elements. Nevertheless, to see that this is really the case is a good check for consistency and if sufficiently many (Coulomb) matrix elements have been kept (because of the necessary truncation discussed above). Figure 4 shows the results obtained for the total density of states from the first and second quantized Hartree calculation. There is a slight difference in absolute energies, i.e. the second quantized Hartree DOS lies slightly below the original, first quantized Hartree result. This is probably due to the necessary truncation of the sum over neighbor shells. Relative to the Fermi level, however, there is nearly perfect agreement so that this consistency check is fulfilled.

The next step beyond the HA is the Hartree-Fock approximation (HFA) which includes the exchange terms in addition to the simple (density-density) Hartree term. The HFA to the Hamiltonian (19) is the effective one-particle Hamiltonian

$$H_{\mathrm{HFA}} = \sum_{12\sigma} \left(t_{12} + \Sigma_{12,\sigma}^{\mathrm{HFA}}\right) c_{1\sigma}^{\dagger} c_{2\sigma} \tag{22}$$

$$\text{with} \quad \Sigma_{12,\sigma}^{\mathrm{HFA}} = \Sigma_{12}^{\mathrm{HA}} - \sum_{34} W_{31,42}^{(sc)} \langle c_{3\sigma}^{\dagger} c_{4\sigma} \rangle. \tag{23}$$

For the exchange part one can use either the unscreened (bare) Coulomb matrix elements or the screened ones. HFA results for the band structure for both cases (screened and unscreened) are shown in Figure 5 and compared with the HA-result shown already in Figure 1 (corresponding to the DOS of Fig. 4). We see that the main effect of the exchange term is to draw the bands downwards again compared to the Hartree result. Within the unscreened HFA the bands are drawn further down than within the screened HFA, because the unscreened matrix elements are larger and the inter-site contributions are also not negligible. Also the total band width is slightly enlarged within the unscreened HFA. Note that we do not observe any (logarithmic) Fermi edge singularities, which are commonly expected for a HFA treatment of quasi-free electron systems. This is due to the fact that we use an effective cutoff (truncation) of our Coulomb matrix elements, because they fall off rapidly with increasing distance from the Wannier function localization center $\mathbf{R}$. This means that – also for the unscreened calculation – our Coulomb interaction is not really long-ranged. The HFA Fermi level singularities (well known from the homogeneous electron gas, for instance [5]) have to be considered as an artefact of the HFA. Therefore, our formulation of HFA starting from a localized basis automatically avoids this artefact because of the effective (necessary) truncation and short ranged nature of the effective Coulomb interaction. On the one-hand side this is an artefact of this additional truncation, on the other hand in reality such a truncation of the effective Coulomb matrix elements (due to screening and correlation effects beyond HFA) exists. Therefore, a HFA formulation not leading to (artificial)

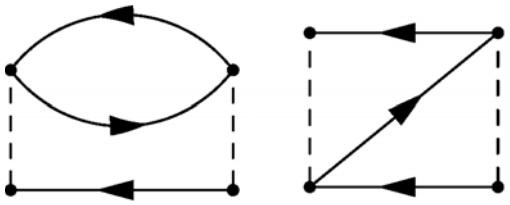

Fig. 6. Two selfenergy Feynman diagrams occurring in second order in the interaction.

singularities may also be considered to be an advantage over standard HFA treatments (in k-space and, therefore, with singularities).

In a screened HFA treatment this problem does not occur, as the screened Coulomb matrix elements really are only short-ranged and a consideration of only the on-site Coulomb matrix elements is sufficient. We see from Figure 5 that the screened HFA essentially only slightly shifts the Hartree bands energetically downwards but qualitatively (and relative to the Fermi energy) is similar to the HA-result (and also the LDA-result, compare Fig. 1).

6 Second order perturbation theory (SOPT) with screened Coulomb matrix elements

The final goal is to take into account true many-body (correlation) effects, and this means to apply systematic many-body theory beyond HFA. From the band structures shown in Figures 1, 5 and the (Hartree) density of states shown in Figure 4 we see that the relevant conduction bands of Li have a band width of about 16−17 eV. From Table 4 we see that the largest (direct on-site) screened Coulomb matrix elements are of the magnitude 2−5 eV, i.e. they are considerably smaller than the band width. Therefore, for the simple metal Li a weak-coupling many-body approximation is justified. The simplest weak-coupling approximation beyond HFA is the second order perturbation theory (SOPT). We neglect all intersite Coulomb matrix elements and the exchange matrix elements, because – according to Table 4 – these are small compared to the on-site intraband (screened) Coulomb matrix element ("Hubbard-U") $U = 4.63$ eV and the on-site inter-band Coulomb matrix element $V = 2.36$ eV. With these two matrix elements we apply SOPT relative to the HFA result. Then, according to standard many body theory [5], the two selfenergy diagrams shown in Figure 6 have to be taken into account in addition to the (screened) HFA-contribution according to (22). In the diagrams the full lines represent HFA Green functions and the dashed lines the matrix elements U and V. An intraband interaction U (between two electrons of different spin at the same site and in the same Wannier state or band) can only occur for the first diagram, whereas the interband interaction V occurs in both diagrams (also spin-diagonal between two electrons of equal spin at the same site but in different bands or Wannier states).

We assume further that the selfenergy is local or **k**-independent, i.e. that only on-site matrix elements (diagonal in real space) are relevant, which is the usual DMFT-assumption [15,16] which is usually good in dimension $d = 3$. Then according to the standard rules of many-body theory these two selfenergy diagrams stand for the analytical expressions

$$\Sigma^{1\sigma}_{nn'}(z) = \sum_{n_1 n_2 \sigma'} u^{\sigma\sigma'}_{nn_1} u^{\sigma\sigma'}_{n'n_2} \int dE_1 \int dE_2 \int dE_3 \times \rho^{\sigma}_{nn'}(E_1)\rho^{\sigma'}_{n_1 n_2}(E_2)\rho^{\sigma'}_{n_1 n_2}(E_3) \times \frac{f(E_1)f(E_2) + f(E_3) - f(E_1)f(E_3) - f(E_2)f(E_3)}{z - E_1 - E_2 + E_3} \tag{24}$$

$$\Sigma^{2\sigma}_{nn'}(z) = \sum_{n_1 \neq n, n_2 \neq n'} u^{\sigma\sigma'}_{nn_1} u^{\sigma\sigma'}_{n'n_2} \int dE_1 \int dE_2 \int dE_3 \times \rho^{\sigma}_{nn_2}(E_1)\rho^{\sigma}_{n_1 n'}(E_2)\rho^{\sigma}_{n_1 n_2}(E_3) \times \frac{f(E_1)f(E_2) + f(E_3) - f(E_1)f(E_3) - f(E_2)f(E_3)}{z - E_1 - E_2 + E_3} \tag{25}$$

with

$$f(E) = \frac{1}{e^{\beta(E-\mu)} + 1}$$

$$u^{\sigma\sigma'}_{nn'} = \begin{cases} 0 \text{ for } n = n' \text{ and } \sigma = \sigma' \\ U \text{ for } n = n' \text{ and } \sigma \neq \sigma' \\ V \qquad \text{for } n \neq n'. \end{cases}$$

Here $\rho^{\sigma}_{nn'}(E)$ denotes the (screened) HFA on-site spectral function (per spin), which has non-diagonal elements with respect to the band indices n, n', in which the maximally localized Wannier functions are obtained. The explicit calculation of the SOPT selfenergy can be greatly simplified using a Laplace transformation of the denominator and an FFT algorithm, as described in reference [30].

Results for the SOPT-selfenergy are shown in Figure 7; real and imaginary part of the (band-index) diagonal element $\Sigma_{nn}(E + i0)$ are shown as thick lines; the thin lines varying around zero (on this linear scale) are the band index off-diagonal contributions, which are at least one magnitude smaller than the main contribution as are the contributions of the second diagram in Figure 6. Obviously, the imaginary part of $\Sigma_{nn}(E+i0)$ vanishes proportional to E^2 exactly at the Fermi energy, reflecting Fermi liquid behavior, which automatically comes out from this approach and is certainly fulfilled for this simple metal. Away from the Fermi energy the selfenergy imaginary part is finite reflecting finite lifetime effects due to the Coulomb scattering. There is also a finite imaginary part at energies below and above the (HFA) band giving rise to a broadening of the DOS when taking into account many-body effects on this level. The real part shows the expected behavior falling off proportional to $1/E$ for large energies

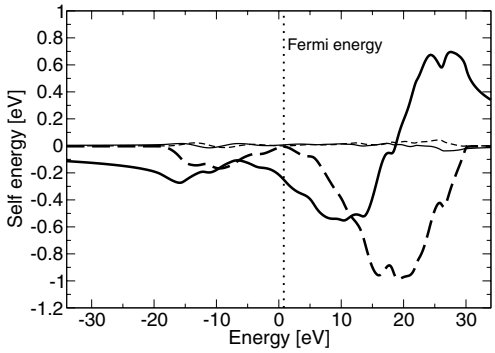

Fig. 7. Energy dependence of SOPT-selfenergy contribution (Fig. 6, relative to screened HFA-result), thick lines: band-index diagonal, thin lines: band-index off-diagonal contributions, dashed lines: imaginary part, full lines: real part.

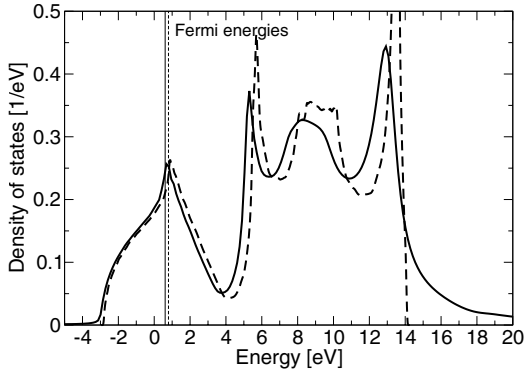

Fig. 8. Density of states for metallic Li obtained in HFA (dashed line) and SOPT (full line).

and some structure within the band. This has to be expected, as it is connected to the imaginary part by the standard Kramers-Kronig relations. The real part of the selfenergy, in particular, has a negative slope at the Fermi level giving rise to a slight mass enhancement due to the Coulomb interaction.

This slope is of the magnitude $\frac{\partial \Sigma}{\partial E} \approx -0.055$ giving rise to a quasiparticle renormalization factor $\frac{m^*}{m} = 1.057$. From the (Hartree, HFA or LDA) band structure shown in Figures 1, 5 one obtains effective band masses at the Fermi energy of the magnitude $m \approx 1.34 - 1.54\, m_0$ in the screened HFA and $m \approx 1.32 - 1.69\, m_0$ in the LDA depending on the direction in k-space (m_0 free electron mass), which is in rough agreement with results obtained previously for Li [31]. Our many-body approximation yields only a slight further mass enhancement due to correlations, which is not yet sufficient to explain values of $m_{th} = 2.19\, m_0$, which can be found in the literature [31,32] for the (thermal) effective mass for Li. This may indicate that the k-dependence of the selfenergy, which contributes to the mass enhancement [5] but is neglected in the DMFT/SOPT used here, is of importance or that despite the fact that we are in the weak-coupling limit higher order resummations of selfenergy diagrams are necessary to obtain a stronger mass enhancement. This and the fact that even for the simple metal Li many-body effects and a quasiparticle mass enhancement cannot be neglected is also in agreement with recent results of a GWA application [33].

Keeping only the (band index) diagonal matrix elements of the selfenergy contribution (24) (corresponding to the first diagram of Fig. 6), the SOPT density of states can be calculated according to

$$\rho_{n\sigma}(E) = \frac{-1}{\pi} \int d\epsilon \rho^0_{n\sigma}(\epsilon) \mathrm{Im} \frac{1}{E + i0 - \Sigma^\sigma_{nn}(E) - \epsilon} \quad (26)$$

where $\rho^0_{n\sigma}(\epsilon)$ denotes the HFA-DOS of the nth band.

In Figure 8 we show this SOPT-DOS and compare it with the HFA-DOS (dashed line). We see that in the main part of the spectrum, in particular in the occupied part, the SOPT yields only a small correction to the HFA-result. There is a slight shift downwards and there are tails in the SOPT-DOS resulting from the finite imaginary part of the selfenergy also in energy regions of still vanishing HFA-DOS. Furthermore, the sharp structures in the unperturbed (Hartree and HFA) DOS are smeared out in SOPT, which again is due to the finite selfenergy imaginary part. But altogether, correlation effects are relatively small, as expected for this simple metal and justifying once more the application of a weak-coupling many-body approximation.

7 Conclusion

We have proposed and applied a new combination of an ab initio (first principles) method with many-body methods. We start from a first-principles Hartree calculation, which yields the Hartree band structure and a suitable one-particle basis in the form of Bloch functions. From the eigenenergies a calculation of the static susceptibility and dielectric function is possible. From the Bloch functions one can determine maximally localized Wannier functions as a new one-particle basis of spatially localized functions. Within this Wannier basis all the one-particle and two-particle (Coulomb) matrix elements can be calculated. This yields the many-body Hamiltonian in second quantization with parameters determined "from first principles". Using the static dielectric function also screened Coulomb matrix elements can be obtained. The simplest approximations to be applied to this second quantized Hamiltonian is again the Hartree and the Hartree-Fock approximation (HFA), which can be applied using screened or unscreened Coulomb matrix elements. Many-body methods beyond HFA can be applied at least when using the second quantized Hamiltonian with the screened Coulomb matrix elements.

To demonstrate the feasibility of this approach we applied it to the simple metal Li. For this system we performed an LMTO band structure calculation in Hartree approximation keeping only the $2s$- and $2p$ ($l = 0, 1$) bands. The maximally localized Wannier functions obtained turn out to be of the sp^3-orbital form and to be localized with a degree of about 96% within the first, central unit cell (muffin-tin sphere). The unscreened Coulomb

matrix elements are still relatively large, of the order of 13 eV for the on-site intraband, of 10 eV for the on-site interband, and still up to 6 eV for the nearest neighbor direct (density-density) Coulomb interaction. The screened Coulomb matrix elements are considerably smaller; we obtain an order of 4 eV for the intraband on-site, 2 eV for the interband on-site and negligible small intersite screened Coulomb matrix elements. Therefore, with screened Coulomb matrix elements the second quantized Hamiltonian is of the form of a four-band Hubbard model with an on-site intraband Hubbard-U and a local (on-site) interband Coulomb matrix element V. As these screened Coulomb matrix elements are small compared to the conduction band width, one is in the weak coupling situation for this simple metal. Therefore, a weak-coupling many-body approximation is justified, and we calculated the electronic selfenergy within second order perturbation theory (SOPT). We obtain Fermi liquid behavior with a small mass enhancement due to the weak correlation effects and only a small modification of the SOPT-density of states when compared to the HFA-result, which once more shows that the weak-coupling theory is sufficient in this case.

But the method used and proposed is, in principle, also applicable to other, more strongly correlated systems. Only the many-body approximation to be applied will be a different one when the screened Coulomb matrix elements are no longer small in comparison to the band width, because then SOPT is probably no longer sufficient. Then other many-body methods, probably based on the DMFT, will have to be applied.

This work has been supported by a grant from the Deutsche Forschungsgemeinschaft No. Cz-31/12-1. We thank Bob Albers for a cooperation in the early stages of this project, for his interest and for useful discussions.

References

1. P. Hohenberg, W. Kohn, Phys. Rev. **136**, B 864 (1964)
2. R.M. Dreizler, E.K.U. Gross, *Density Functional Theory*, Springer (Berlin, Heidelberg, New York, 1990)
3. H. Eschrig, *The Fundamentals of Density Functional Theory* (Teubner Stuttgart, Leipzig, 1996)
4. W. Kohn, L.J. Sham, Phys. Rev. **140**, A1133 (1965)
5. G.D. Mahan, *Many-Particle Physics* (Plenum Press New York, 1990)
6. V.I. Anisimov, J. Zaanen, O.K. Andersen, Phys. Rev. B **44**, 943 (1991)
7. M.M. Steiner, R.C. Albers, L.J. Sham, Phys. Rev. B **45**, 13272 (1992); Phys. Rev. Lett. **72**, 2923 (1994)
8. V.I. Anisimov, A.I. Poteryaev, M.A. Korotin, A.O. Anokhin, G. Kotliar, J. Phys. Cond. Matter **9**, 7359 (1997)
9. A.I. Lichtenstein, M.I. Katsnelson, Phys. Rev. B **57**, 6884 (1998)
10. A. Liebsch, A. Lichtenstein, Phys. Rev. Lett. **84**, 1591 (2000)
11. I.A. Nekrasov, K. Held, N. Blümer, A.I. Poteryaev, V.I. Anisimov, D. Vollhardt, Eur. Phys. J. B **18**, 55 (2000)
12. A.I. Lichtenstein, M.I. Katsnelson, G. Kotliar, Phys. Rev. Lett. **87**, 067205 (2001)
13. L. Chioncel, L. Vitos, I.A. Abrikosov, J. Kollar, M.I.Katsnelson, A.I. Lichtenstein, Phys. Rev. B **67**, 235106 (2003)
14. A. Georges, G. Kotliar, W. Krauth, M.J. Rozenberg, Rev. Mod. Phys. **68**, 13 (1996)
15. G. Kotliar, D. Vollhardt, Physics Today **57**(3), 53 (2004)
16. K. Held, I.A. Nekrasov, G. Keller, V. Eyert, N. Blümer, A.K. McMahan, R.T. Scalettar, T. Pruschke, V.I. Anisimov, D. Vollhardt, Psi-k Newsletter **56**, 65 (2003)
17. P.H. Dederichs, S. Blügel, R. Zeller, H. Akai, Phys. Rev. Lett. **53**, 2512 (1984)
18. H. Meider, M. Springborg, J. Phys.: Condens. Matt. **10**, 6953 (1998)
19. L. Hedin, B.I. Lundquist, Solid State Physics **23**, 1, edited by F. Seitz, D. Turnbull, H. Ehrenreich (Academic Press, 1969)
20. F. Aryasetiawan, O. Gunnarsson, Rep. Prog. Phys. **61**, 237 (1998)
21. W. Aulbur, L. Jönsson, J.W. Wilkins, Solid State Physics **54**, 2, edited by H. Ehrenreich, F. Spaepa (Academic Press, 2000)
22. F. Aryasetiawan, O. Gunnarsson, Phys. Rev. B **49**, 16214 (1994)
23. S. Biermann, F. Aryasetiawan, A. Georges, Phys. Rev. Lett. **90**, 086402 (2003); F. Aryasetiawan, M. Imada, A. Georges, G. Kotliar, S. Biermann, A.I. Lichtenstein, Phys. Rev. B **70**, 195104 (2004)
24. N. Marzari, D. Vanderbilt, Phys. Rev. B **56**, 12847 (1997)
25. I. Schnell, G. Czycholl, R.C. Albers, Phys. Rev. B **65**, 075103 (2002)
26. I. Schnell, G. Czycholl, R.C. Albers, Phys. Rev. B **68**, 245102 (2003)
27. O.K. Andersen, Phys. Rev. B **12**, 3060 (1975)
28. H.L. Skriver, *The LMTO Method* (Springer-Verlag, Heidelberg, 1984)
29. U. von Barth, L. Hedin, J. Phys. C **5**, 1629 (1972)
30. H. Schweitzer, G.Czycholl, Z. Phys. B – Cond. Matter **79**, 377 (1990)
31. W.Y. Ching, J. Callaway, Phys. Rev. B **9**, 5115 (1974)
32. D.L. Martin, Proc. R. Soc. A **263**, 378 (1961)
33. Y. Kubo, J. Phys. Soc. Jpn **66**, 2236 (1997)